H3K27me3-rich genomic regions can function as silencers to repress gene expression via chromatin interactions

Yichao Cai[1]*, Ying Zhang[2]*, Yan Ping Loh[2], Jia Qi Tng[2], Mei Chee Lim[2,3], Zhendong Cao[2,4], Anandhkumar Raju[5], Shang Li[3,6], Lakshmanan Manikandan[5], Vinay Tergaonkar[5], Greg Tucker-Kellogg[1,8†], Melissa Jane Fullwood [2,5,9†]

[1]Department of Biological Sciences, National University of Singapore, 16 Science Drive 4, 117558 Singapore.
[2]Cancer Science Institute of Singapore, National University of Singapore, 14 Medical Drive, 117599 Singapore.
[3]Cancer and Stem Cell Biology Programme, Duke-NUS Medical School, 8 College Road, 169857 Singapore.
[4]Department of Cancer Biology, Perelman School of Medicine, University of Pennsylvania, Philadelphia, PA19104, USA.
[5]Institute of Molecular and Cell Biology, Agency for Science, Technology and Research (A*STAR), 61 Biopolis Drive, Proteos, 138673 Singapore.
[6]Department of Physiology, Yong Loo Lin School of Medicine, National University of Singapore, 2 Medical Drive,117597 Singapore.
[7]Department of Pathology, National University Health System, 1E Kent Ridge Road, 119228 Singapore.
[8]Computational Biology Programme, National University of Singapore, 6 Science Drive 2, 117546 Singapore
[9]School of Biological Sciences, Nanyang Technological University, 60 Nanyang Drive, 637551 Singapore.

*These authors made equal and critical contributions
[†]Correspondence should be sent to:
(1) Melissa J. Fullwood, Cancer Science Institute Singapore (CSI) and School of Biological Sciences, Nanyang Technological University, Email: mfullwood@ntu.edu.sg; Telephone: (65) 6516 5381; Fax: (65) 6873 9664
(2) Greg Tucker-Kellogg, Department of Biological Sciences, National University of Singapore. Email: dbsgtk@nus.edu.sg, Telephone: (65) 6516 4740

Abstract

Gene repression and silencers are poorly understood. We reasoned that H3K27me3-rich regions (MRRs) of the genome defined from clusters of H3K27me3 peaks may be used to identify silencers that can regulate gene expression via proximity or looping. MRRs are associated with chromatin interactions and interact preferentially with each other. MRR-associated genes and long-range chromatin interactions are susceptible to H3K27me3 depletion. MRR component removal at interaction anchors by CRISPR leads to upregulation of interacting target genes, altered H3K27me3 and H3K27ac levels at interacting regions, and altered chromatin interactions. Chromatin interactions did not change at regions with high H3K27me3, but regions with lower H3K27me3 and higher H3K27ac levels showed losses in chromatin interactions, while new interactions emerged at high H3K27ac regions. The MRR knockout cells also showed changes in phenotype associated with cell identity, and altered xenograft tumor growth. Our results characterize H3K27me3-rich regions and their mechanisms of functioning.

Introduction

The 3-dimensional organization of our genomes is important for gene regulation[1-3]. The genome is organized into large Topologically-Associated Domains (TADs) and chromatin interactions. Gene transcription is controlled by transcription factors (TFs) that bind to enhancers and promoters to regulate genes[4]. TFs can bind to proximal enhancers in the genome, and enhancers distal to genes can loop to gene promoters via chromatin interactions to activate gene expression[3]. Cancer cells show altered chromatin interactions[2,3] including altered chromatin loops to key oncogenes such as *TERT*[5].

By contrast, mechanisms for gene repression are much less well understood. Silencers are regions of the genome that are capable of silencing gene expression. Silencers have been shown to exist in the human genome, but are less well characterized than enhancers. Until now, there are only a few known experimentally validated silencers that have been demonstrated to repress target genes *in vitro*, such as the human synapsin I gene[6], the human *BDNF* gene[7] and human *CD4* gene[8,9] (experimentally validated silencer examples are discussed in Table S1). The reason for the lack of known silencers in the literature is that methods that can identify human silencer elements in a genome-wide manner are not fully developed yet. Moreover, the mechanism by which silencers can regulate distant genes is still uncharacterized. Distant silencers are thought to loop over to target genes to silence them[10,11], and this has been demonstrated in studies of polycomb-mediated chromatin loops in *Drosophila*[12] and in mice[13], but no such examples have been characterized to date in humans.

Polycomb Group (PcG) proteins including Polycomb Repressive Complexes, PRC1 and PRC2 are widely recognized to mediate gene silencing of developmental genes[14]. During the development process, PRC1 and PRC2 have the ability to orchestrate genome architecture and repress gene expression[15]. There are two different types of expression domains: active domain and repressive domain, which to regulate gene expression and construct cellular identity. Genes involved in cell self-renewal are contained within the active domains which governed by super-enhancers, while genes specifying repressed lineage are organized within chromatin structures known as PcG domains[16]. Moreover, intact PcG domains have been showed necessary to maintain the chromatin interaction landscape[17,18]. However,

the mechanisms of PcG domain formation and PcG protein recruitment are not fully characterized yet[19] which makes finding silencers more difficult.

PcG domains are marked by H3K27me3, which is deposited by the catalytic component of PRC2 complex, mainly Enhancer of zeste homolog 2 (EZH2) and sometimes EZH1[20]. H3K27me3 marks are associated with gene repression for cell type-specific genes. Unlike H3K9me3 which remains silenced all the time and prevents multiple TFs from binding[21], H3K27me3 still allows these genes to be activated through TF binding in a different cell state[22]. H3K27me3 are known to be a characteristic of silencers[18,23].

Recently, there are several papers that have proposed methods to identity silencer elements in genome-wide manners. Huang *et al* defines silencers using the correlation between H3K27me3-DNase I hypersensitive site (DHS) and gene expression[24]. At the same time, Jayavelu *et al* used a subtractive analysis approach to predict silencers in over 100 human and mouse cell types[25]. Moreover, Pang and Snyder identified silencers through an innovative "ReSE screen" which screened for genomic regions that can repress caspase 9 expression upon apoptosis induction[26]. Interestingly, Ngan *et al.* characterized silencers in mouse development through PRC2 Chromatin Interaction Analysis with Paired-End Tag sequencing (ChIA-PET) in mouse embryonic stem cells. They concluded that PRC2-bound anchors function as transcriptional silencers suggesting that we can identify silencers through investigating chromatin interactions[13].

However, there is no consensus yet in terms of how to identify silencers – notably, each of these methods identify different genomic regions as silencers, raising the question of whether there may be different classes of silencers. Moreover, current methods for identifying silencers are laborious and require complicated bioinformatics analyses and/or genome-wide screening (Table S2, "comparison of different human silencer identification methods"). A simple, easy to perform method to identify silencers in the genome in a high-throughput manner would be ideal. Further, we need more research in order to understand whether there are different classes of silencers and to characterize the roles of silencers in the genome.

The term "super-enhancer"[27] has been used to describe clusters of H3K27ac peaks which show very high levels of H3K27ac or other transcription-associated factors such as mediator as determined from ChIP-Seq data. Super-enhancers have high levels of chromatin interactions to target genes[28], and are associated with oncogenes in cancer cells[29] and cell fate-associated genes in embryonic stem cells[30]. While more research needs to be done to determine if super-enhancers are a distinctly different entity from enhancers, super-enhancers are thought of as strong enhancers, and the definition has been useful in identifying genes important for cell-type specification[31].

Here, we reasoned that we can similarly identify "super-silencers" or "H3K27me3-rich regions (MRRs)" from clusters of H3K27me3 peaks in the genome through ChIP-Seq on H3K27me3. We hypothesized that H3K27me3-rich regions may be a useful concept in identifying genomic regions that contain silencers which can repress target genes either in proximity or via long-range chromatin interactions. The target genes may be tumor suppressors in cancer cells, and also cell fate-associated genes that need to be turned off for differentiation to occur.

We found several hundred MRRs in the K562 chronic myelogenous leukemia cell line, which show dense chromatin interactions to target genes and to other MRRs. Moreover, genes in close proximity to, and genes that loop to MRRs by long-

range chromatin interactions, were more susceptible to EZH2 inhibition and showed higher levels of upregulation upon EZH2 inhibition, as compared with genes in close proximity or which loop to typical H3K27me3 peaks. EZH2 inhibition led to changes in long-range chromatin interactions at MRRs. Next, we experimentally validated two looping silencers through CRISPR removal, and both showed upregulation of target genes indicating that they are indeed *bona fide* silencers. Through CRISPR excision of one of the *IGF2* looping silencer components and one of the *FGF18* looping silencer components, we found that silencers control cell identity and their removal caused cell identity changes. Using the silencer at *IGF2* as an example, we dissected the consequences of silencer removal through 4C and ChIP-Seq on H3K27me3 and H3K27ac. We found that removal of a component of a silencer by CRISPR excision leads to changes in chromatin loops. Remarkably, regions that originally presented with very high H3K27me3 levels were stable in terms of chromatin loops. New chromatin interactions formed at regions with high H3K27ac, while chromatin interactions to regions with low H3K27me3 and medium H3K27ac levels were lost.

Taken together, our results indicate that clustering of H3K27me3 peaks in a manner similar to the super-enhancer analyses can identify MRRs that contain silencers that can loop over to target gene promoters, and the epigenomic, transcriptomic and phenotypic consequences of silencer perturbation by H3K27me3 depletion and CRISPR excision.

Results

Identification and characterization of H3K27me3-rich regions (MRRs) in the human genome

We identified highly H3K27me3-rich regions (MRRs) from cell lines using H3K27me3 ChIP-seq data[32] in the following manner: we first identified H3K27me3 peaks, then clustered nearby peaks, and ranked the clustered peaks by average H3K27me3 signals levels. The top clusters with the highest H3K27me3 signal were called as “H3K27me3-rich regions” (MRRs) and the rest “typical H3K27me3” regions (Figure 1A, 1B). The peaks that were merged together during this process were called constituent peaks. This method is similar to how super-enhancers were defined[30,33]. We overlapped our list of MRRs in K562 with a recent paper[26] which performed whole genome silencer element screening and found that 41% of our MRRs overlap with the list of silencer elements defined by the ReSE screen[26] (Figure S1A), indicating that our MRRs could identify silencers in the genome.

The number of constituent peaks and overlapping genes at MRRs is larger than typical H3K27me3 peaks (Figure S1B, S1C). Consider the differences in the lengths of MRRs and typical H3K27me3 peaks, we used constituent peaks of MRRs and typical H3K27me3 peaks to study CpG methylation and gene features. The results showed that the constituent peaks of MRRs and typical H3K27me3 peaks mostly overlap with inter CpG island methylation (Figure S1D) and the intronic regions of genes (Figure S1E).

Many MRR-overlapping genes in different cell lines are known or predicted tumor suppressor genes[34] (Figure S1F). For example, *NPM1*, the most commonly mutated gene in leukemia[35-38], overlaps with an MRR in the leukemic cell line K562. *FAT1*, which is frequently mutated in chronic lymphocytic leukemia (CLL) and can act as a tumor suppressor through inhibiting Wnt signaling[39,40], also overlaps with an MRR in K562. Gene ontology analysis showed that MRR-related genes are enriched

in developmental and differentiation processes, while genes associated with typical H3K27me3 peaks are enriched in cell metabolism and transportation processes (Figure S1G, S1H). These results suggest that MRR may regulate important genes related to development and tumorigenesis.

ChIP-seq signals of EZH2 showed high correlation with H3K27me3 signal at typical H3K27me3, MRRs, constituent peaks of typical H3K27me3 and constituent peaks of MRRs, which is consistent with EZH2's role in H3K27me3 mark deposition (Figure 1C; Figure S1I, S1J). Notably, the constituent peaks of MRRs had higher H3K27me3 and EZH2 signals than the constituent peaks of typical H3K27me3 peaks. This suggests that there are genomic regions with higher level of H3K27me3 and EZH2 compared with others, and they can be found in MRRs. In addition, the ChIP-seq profiles of SUZ12 and BMI1 are also higher in the constituent peaks of MRRs, suggesting that these regions may be targeted by PRC1 and PRC2 complex (Figure S1K, S1L).

MRRs were different in different cell lines, where a same gene can overlap with different types of peaks (Figure 1D; S1M, S1N). For example, the cadherin-like coding gene *CPED1* is covered by a broad MRR in GM12878, but overlaps with a super-enhancer in K562 (Figure 1D). Conversely, the gene for *DENND2D* is associated with an MRR but overlaps with a super-enhancer in GM12878 (Figure 1D). In addition, most MRRs were unique to individual cell lines (Figure S1Q).

Analysis of cell line expression data showed that genes which transit from MRR-associated to H3K27ac peak-associated in a different cell line were up-regulated, while genes transit from super enhancer-associated to H3K27me3 peak-associated were down-regulated (Figure 1E). The expression fold changes between repressive and active state are higher than those genes that merely lost MRR/SE (Figure 1E; MRR vs. others and SE vs. others) or gain H3K27ac/H3K27me3 (Figure 1E; others vs. H3K27ac and others vs. H3K27me3), respectively. Further, genes whose expression was more cell line-specific were associated with more MRRs than those genes with lower expression specificity (Figure S1R). The uniqueness and specificity of MRRs suggest they might be primed for specific regulation in different cell contexts.

We overlapped MRRs with high-resolution *in situ* Hi-C data[41], and found that constituent peaks of MRRs had a higher density of chromatin interactions than the constituent peaks of typical H3K27me3 peaks in both K562 and GM12878 (Figure 1F; Figure S1N, S1O). The involvement of chromatin interactions in MRRs was similar to super-enhancers compared with typical enhancers[42], suggesting chromatin interactions might be important within strong histone modification regions.

In summary, we defined MRRs using H3K27me3 ChIP-seq peaks, and showed that MRRs might be involved with specific gene repression related to development, differentiation and cancer via chromatin interactions.

H3K27me3-rich regions (MRRs) preferentially associate with MRRs in the human genome via chromatin interactions

We assigned chromatin states at Hi-C interaction anchors using H3K27me3 and H3K27ac peaks: active (A) anchors overlap with H2K27ac peaks, repressive (R) anchors overlap with H3K27me3 peaks, bivalent (B) anchors overlap with both H3K27me3 and H3K27ac peaks, and quiescent (Q) anchors overlap with neither peak (Figure 2A). We further defined the chromatin state pair of an interaction as the chromatin states of its anchors and calculated the proportion of different chromatin interaction in the Hi-C data (Figure 2B, “Obs”). Next, we calculated the expected

proportion of interactions for each state pair under a homogeneous model (Figure 2B, Exp), and compared those expectations to the actual number of observations (Figure 2B, $\log_2$(Obs/Exp) on the x-axis). If the observed proportion of a certain category of interactions were more frequently seen, the $\log_2$(Obs/Exp) value would be positive; conversely, if a certain category was depleted, the $\log_2$(Obs/Exp) value would be negative.

Interactions between anchors of the same state (AA, RR, and BB) were more likely to interact with each other, while interactions with highly different chromatin state pairs (e.g., AR, BQ) less likely (Figure 2B, left), regardless of cell line. When grouped into typical H3K27me3 peaks (T) versus high H3K27me3 regions or MRRs (MRR), the high H3K27me3 regions showed a preference for interactions with other MRRs (Figure 2B, right). In keeping with A/B chromatin compartments of the nucleus, this 'like-like' preference indicated that loci of similar chromatin state were more prone to interact with each other.

To further explore the potential regulatory role of MRRs in chromatin interactions, we identified the subset of MRR-anchored interactions where at least one anchor peak overlapped a gene transcription start site, and grouped them according to whether the MRR anchor was proximal or distal to the TSS anchor (Figure 2C, 2D; Figure S2A-S2F, S2G; examples of genes can be found in Figure S2H-S2K). Both proximal and distal gene looping occur for MRR-anchored interactions, but some MRRs are large enough that both anchors occur in the same MRR. While proximal looping genes are a subset of the genes within MRRs, distal looping genes are only identified by chromatin interactions (Figure 2D, right). The top-ranking MRRs are often involved in extensive internal looping (Figure S2J-S2K). Gene ontology analysis showed that MRR-associated genes in the context of chromatin interactions are involved in developmental and differentiation processes (Figure S2L).

In order to validate the ‘like-like’ preference of chromatin interactions, we performed Circular Chromosome Conformation Capture (4C) experiments on selected loci at MRR to investigate the associated chromatin interactions in a comprehensive and high-resolution manner. We annotated the interactions based on the chromatin state of the anchor distal from the bait in K562 (Figure 2E and Figure S2M-O), and across multiple cell lines (Figure S2P-Q). The interaction profiles of 4C baits of different states were largely dominated by interacting regions of the same state as the baits. In addition, the *TMCO4* 4C data showed that most 4C interactions fell within the same MRR as the bait and only a handful of them were outside of the MRR. This suggest that MRR can have extensive internal looping.

We also carried out 4C experiments on the same bait across different cell lines. The interactions and the chromatin state at the bait locus varied in different cell lines, but the interaction profile maintained a preference for the same chromatin state as the bait (Figure S2P, S2Q). As a further test of this concept, the extensive BB long-range interactions (green arcs) connecting *PSMD5* and *TOR1A* in K562 were validated using reciprocal 4C bait design. When the *PSMD5* bait region was A (active) in either GM12878 or HAP1 cells, the BB interactions were largely reduced and other types of interactions started to appear (Figure S2P).

Next, we analyzed the transcription factors binding to the regions of MRRs that are connected by chromatin interactions. ChIP-seq peaks of chromatin architectural proteins (CTCF, YY1, ZNF143), cohesin subunits (RAD21, SMC3), and transcription repression-associated proteins (EZH2, REST, GATAD2B) were downloaded from ENCODE and overlapped with the interacting regions of MRRs,

which were then normalized to Z-score and clustered by hierarchical clustering. Specific enrichments of one specific transcription factor can be found in several small clusters (Figure 2F; YY1 in cluster_1, EZH2 in cluster_2, and SMC3 in cluster_3). Another cluster was identified with very high binding affinity of RAD21, REST, ZNF143, CTCF, and SMC3 (Figure 2F cluster_5). Our results demonstrate that different chromatin architectural proteins are involved in the regulation of different silencer-associated chromatin interactions.

MRR-associated gene expression and long-range chromatin interactions are susceptible to EZH2 perturbation

In order to investigate the effects of H3K27me3 on MRR-associated chromatin interactions and associated gene expression, we eliminated or reduced H3K27me3 by CRISPR knock-out of EZH2 in HAP1 cells (a near haploid cell line derived from chronic myeloid leukemia) and EZH2 inhibitor treatment (GSK343) in K562 cells.

After treatment with GSK343 in K562 cells, the level of H3K27me3 decreased globally, leading to the loss of nearly half of the H3K27me3 ChIP-seq peaks (Figure 3A). However, there were still residual H3K27me3 peaks after GSK343 treatment, and these were the regions that had higher H3K27me3 signal before the treatment as compared with the susceptible peaks. Western blot confirmed that a lower concentration of drug treatment in K562 cells and EZH2 knockout in HAP1 cells both led to global loss of H3K27me3 (Figure S3A-B).

To interrogate the gene expression changes of MRR-related genes, we performed RNA-seq in DMSO-treated and GSK343-treated K562 cells. The RNA-seq results indicated strong up-regulation of H3K27me3-associated genes, while genes associated with H3K27ac peaks (super enhancers or typical enhancers) underwent minimal net change (Figure 3B). Notably, MRR-associated genes were the most strongly upregulated as compared with other categories (typical H3K27me3, super-enhancer and typical enhancers) (Figure 3B). Similarly, a lower dose of drug treatment in K562 and EZH2 knockout in HAP1 also induced H3K27me3 depletion and significant up-regulation of MRR-associated genes as compared with other categories (Figure S3C-E). In addition, cell adhesion related genes in RNA-seq of HAP1 and K562 cells were significantly up-regulated (Figure S3F-S3I). This is in concordance with the increased aggregation HAP1 EZH2 KO cells (Figure S3J). HAP1 EZH2 KO cells also expressed slower growth rate compared with EZH2 WT cells (Figure S3K), possibly due to contact inhibition of the cells. Taken together, our results showed that MRR-associated genes were highly susceptible to EZH2 inhibition and cell adhesion pathways were up-regulated.

Based on the genes that were up-regulated following H3K27me3 depletion, we selected candidate MRR-associated genes to examine whether their interactions had been changed by EZH2 inhibition. ChIP-seq data at *FGF18* gene showed that H3K27me3 level was decrease and there were accompanied lost peaks, while the H3K27ac and H3K4me3 signal were mostly unaltered (Figure 3C). By comparing the 4C interactions at *FGF18* promoter in DMSO and GSK343 condition, we found that 4C interactions at near distance stayed almost the same (Figure 3D, 50 kb range view on the left), while interactions with greater genomic spans were altered (Figure 3D, 1000 kb range view on the right). We further classified 4C interactions into “gained”, “lost”, and “unchanged” categories, and showed that the unchanged 4C interactions showed a closer distance relative to the 4C bait compared with gained or lost categories (Figure 3E). This trend was observed in all of the 4C libraries of in

GSK343-treated K562 cells (Figure 3F; Figure S3L) as well as HAP1 EZH2 KO cells (Figure S3L, for details of 4C interactions see Figure S3M-S3S). One question is whether the reduced 4C signal upon H3K27me3 depletion is due to a reduced number of cells displaying chromatin interactions at MRRs. The HAP1 cell line is near-haploid, therefore we can conclude that the reduced 4C signal seen in the HAP1 cells indicates that reduced numbers of cells display these interactions (Figure S3L, Figure S3M-S3S).

Similarly, chromatin interactions of other 4C experiment genes were largely unaffected in the vicinity of the 4C bait (Figure S3M-S3S). Taken together, these results showed that short-range chromatin interactions stayed highly similar upon depletion of H3K27me3, while long-range chromatin interactions are changed by EZH2 inhibition and/or knockout.

CRISPR excision of a silencer looping to *FGF18* leads to *FGF18* gene upregulation, cell differentiation and tumor growth inhibition

Next, we asked if MRRs function as silencers to regulate gene expression. We selected 2 MRRs for functional testing based on the H3K27me3 signal, the presence of Hi-C anchors and the number of Hi-C anchors they associated with whether the genes were involved in cell identity (Supplementary Text). Briefly, there are 974 MRRs in K562 (Figure S4A) and of those MRRs, 237 MRRs are associated with genes. Among these, 130 MRRs show proximal looping to genes (MRRs overlap with target gene promoters), 111 MRRs show distal looping to genes (MRR loops over to the promoter of target gene by long-range chromatin interactions) and 51 MRRs show internal looping to genes (Part of the MRR overlaps with the target gene promoter and the other part of the MRR loops over to the promoter of the target gene by long-range chromatin interactions). From this list, we selected MRR1, an internal looping example which showed many loops to *FGF18*, a fibroblast growth factor involved in cell differentiation and cell-to-cell adhesion[43,44] (Figure 4A) and MRR2, an internal looping example which showed many loops to *IGF2*, an imprinted gene known to be associated with genomic silencers[45] and involved in growth, development and cancer[46] (Figure 5A).

We designed the CRISPR deletion site at a 1 kb region in MRR1 (termed "MRR1-A1") located in the *FBXW11* intronic region that was associated with one of two Hi-C anchors that loop over to *FGF18* (Figure 4A). This region has high H3K27me3 as validated by ChIP-qPCR (Figure S4B). MRR-A1 is part of cluster_8 (associated with low levels of cohesin proteins, high binding to GATAD2B; Table S8) from Figure 2F. We performed 4C using MRR1-A1 as the viewpoint to detect all the genomic locations that have chromatin interactions with this region in wild-type K562. The 4C-seq results showed that this region indeed had chromatin interactions with *FGF18* and several other genes such as *NPM1* and *UBTD2* (Figure 4A).

Next, we performed CRISPR deletion and generated three knock out (KO) clones (Figure S4C). To scan for the target genes, we aligned RNA-seq data of one KO clone and 4C-seq data (Figure 4A) and found that *FGF18* and *UBTD2* were both upregulated upon CRISPR deletion. Upregulation of the *FGF18* gene was further confirmed by RT-qPCR consistently in three different KO clones (Figure 4B) which indicated that MRR1-A1 removal leads to upregulation of *FGF18* gene expression. To confirm that upregulation of *FGF18* was due to H3K27me3 removal, we treated the control cells and KO cells with GSK343 (EZH2 methyltransferase inhibitor). Upon GSK343 treatment, *FGF18* gene was upregulated compared with DMSO control and MRR1-A1 removal can rescue the transcriptional upregulation of *FGF18* (Figure 4C).

Therefore, MRR1-A1 can act as a silencer repressing *FGF18* gene expression via chromatin looping in K562. To explore if this looping silencer is cell type specific, we called MRRs in seven cell lines and found *FGF18* MRR is specific to two of the seven cell lines, K562 and GM12878 (Figure S4D) which suggested that silencers are specific to different cell types and might control the cell identity related genes.

Since *FGF18* has been reported to be involved in cell differentiation and cell-to-cell adhesion[44,45], next we asked if KO cells showed any phenotype. To address this, we performed gene ontology (GO) analysis which showed that KO cells may undergo cell adhesion and cell differentiation (Figure 4D). First, we observed that the KO cells show increased adhesion to the cell culture plate surface and formed aggregates while wild type cells are suspension cells (Figure 4E). The adhesion ability was further quantified by cell adhesion assay (Figure 4F). Second, those similar aggregates morphology was reported by some publications[47,48] which showed that aggregates are associated with cell differentiation such as erythroid and megakaryocyte lineage of K562 cells. Therefore, we checked the expression of hemoglobin genes which can be the indicator of erythroid lineage differentiation[49] in the RNA-seq data and further confirmed some of their upregulation (*HBB*, *HBZ* and *HBE1*) by RT-qPCR (Figure 5A). To rescue the erythroid differentiation phenotype, we performed siRNA knock down of *FGF18* gene in the KO cells. Hemoglobin genes can be partially rescued by *FGF18* knock down (Figure 5B) which suggested that erythroid differentiation is indeed caused by *FGF18* upregulation (Figure 5C).

Leukemic cell differentiation induction is associated with cell growth inhibition and small molecule inhibitors such as All-*trans* Retinoic Acid (ATRA) that can induce differentiation have been useful in treatment of Acute Promyelocytic Leukemia, suggesting that methods to induce differentiation could lead to potential leukemia treatments[49,50]. Therefore, we asked if silencer KO is associated with growth inhibition *in vivo*, given that silencer KO leads to cell differentiation. To test this, we performed xenograft experiments for two different KO clones and both two KO clones showed inhibition of tumor growth in the mice (Figure 5D and 5E). This tumor growth inhibition suggests that *FGF18* might play tumor suppressor roles in leukemia and suggests the possibility that silencers can control cell identity through repression of tumor suppressor gene expression. In summary, our analyses suggested MRR1-A1 can function as a looping silencer of *FGF18* and MRR1-A1 removal leads to cell identity changes such as cell adhesion, cell differentiation and tumor growth inhibition (Figure 5C).

CRISPR excision of a silencer looping to *IGF2* leads to *IGF2* gene upregulation, cell differentiation and tumor growth inhibition

MRR2 was validated in the same manner as MRR1. Specifically, we designed another 1 kb deletion in MRR2 (termed “MRR2-A1”) located in an intergenic region 10 kb away from the long non-coding RNA *H19* that was associated with one of three Hi-C anchors that loop over to *IGF2* (Figure 6A). High H3K27me3 signal of MRR2-A1 was confirmed by ChIP-qPCR (Figure S5A) and chromatin interactions to *IGF2* were confirmed by 4C-seq (Figure 6A). MRR2-A1 anchor was in cluster_5 in Figure 2F, and it has high binding affinity of CTCF, RAD21, SMC3 and REST (Table S8).

RT-qPCR in CRISPR KO cells (Figure S5B) and vector control cells showed that *IGF2* was upregulated in all three KO cells (Figure 6B) while H19 only showed upregulation of one KO clone (Figure S6C) indicating MRR2-A1 can function as the looping silencer to repress *IGF2* in K562. Again, *IGF2* was upregulated upon

GSK343 treatment which further can be rescued by MRR2-A1 removal confirmed *IGF2* upregulation is due to H3K27me3 removal (Figure 6C). Similar to MRR1, this *IGF2* looping silencer was also cell type specific (Figure S5D).

We performed RNA-Seq on the MRR2-A1 KO cells as compared with empty vector cells, and in Gene Ontology analysis, we found the term for "cell differentiation" (Figure 6D). Thus, we asked if those KO cells are also undergoing erythroid differentiation. We checked the same hemoglobin genes. We found the haemoglobin genes (*HBB*, *HBZ* and *HE1*) were upregulated in the KO cells (Figure 6E) and their upregulation can be rescued by *IGF2* siRNA knock down (Figure 6F).

Finally, we tested to see whether the CRISPR KO cells showed tumor growth inhibition *in vivo*, similar to MRR1. Xenograft experiments showed severe tumor growth inhibition of two different clones (Figure 6G) which further suggests that silencers can control cancer growth. Therefore, this I*GF2* example together with *FGF18* example confirmed the existence of two looping silencers and showed that looping silencers are involved in the control of cell identity and tumor growth.

IGF2 looping silencer removal caused changes of distant chromatin interactions

Through the *FGF18* and *IGF2* example, we confirmed the existence of looping silencers and demonstrated they can control cell identity. Next, we investigated the epigenomic consequences of removal of a looping silencer using the *IGF2* example. First, we asked whether chromatin interaction landscape will be changed upon looping silencer removal. We performed 4C-seq in the KO cells and control cells. Using *IGF2* as the bait, we detected there are 33 chromatin interactions lost and 12 chromatin interactions gained after knocking out while a control bait remains highly unchanged (Figure 7A, Figure S6A). We further confirmed several lost loops by 3C-PCR (Figure S6B). Taken together, our results indicate that loss of a silencer through CRISPR excision could lead to alterations in the chromatin interaction landscape.

Next, we classified chromatin interactions into three types: unchanged loops, gained loops and lost loops to explore their features. Through mapping their distance and density, we found that the average distance of changed loops are greater than unchanged loops which indicate that the distant loops which are further away to the bait tend to change (Figure 7B), which is consistent with the H3K27me3 depletion experiments (Figure 3E-F).

Chromatin loops to high H3K27ac regions were gained upon *IGF2* looping silencer removal

MRR2 has high H3K27me3 signal, therefore, histone modifications may play a role for the *IGF2* upregulation. We performed H3K27me3 and H3K27ac ChIP-seq in the KO cells and control cells (Figure S6C). We found that H3K27me3 decreased along *IGF2* gene region in the KO cells (Figure 7C) while a control region remained similar (Figure S6D). This suggested that silencer removal will cause H3K27me3 loss at the target gene region.

Next, we performed integrative analysis of 4C-seq and ChIP-seq. Surprisingly, we found that the initial histone states of the cells before knockout were associated with whether the chromatin interactions would be gained, lost or unchanged upon knockout of MRR2-A1 (Figure 7D). Specifically, very repressed loops with high H3K27me3 and low H3K27ac were unchanged and retained after KO. Loops with

high H3K27ac and low H3K27me3 tend to be gained while loops with medium H3K27ac and medium H3K27me3 tend to be lost.

Moreover, in examining the unchanged loops, we observed a slight decrease in H3K27me3 while levels H3K27ac remained similar (Figure S6E) which suggested that the repressive ability of those anchors became weaker.

Taken together, the regions that loop to *IGF2* in the KO cells are now more active with higher H3K27ac regions. These findings demonstrate two mechanisms by which I*GF2* might be upregulated in KO cells. First, *IGF2* showed gains of chromatin loops to more active anchors and losses of loops to several repressive anchors. Secondly, the retained loops which had strong H3K27me3 levels at the control cells show weaker H3K27me3 levels now (Figure 7E).

Discussion

Silencers are important regulatory elements for gene regulation, and several studies have suggested that they loop to target genes, in a manner analogous to enhancers. Although there are several silencer examples that have been experimentally validated (Table S1) and several methods have been proposed to identify silencer elements (Table S2), however, there is no consensus yet. Additionally, no silencers that work via a looping mechanism have been characterized yet except several PRC2-bound silencers in mouse[13]. Here, we propose a new method to identify H3K27me3-rich regions (MRRs) or putative "super-silencers" through clustering and ranking H3K27me3 signals.

In this way, we found that MRRs are highly associated with chromatin interactions and can be perturbed by EZH2 inhibition. Through H3K27me3 clustering, ranking and associate them with chromatin interactions, we validated two looping silencer examples (*IGF2* and *FGF18* examples). We showed that silencer removal cause cell identity changes and further related to tumor growth inhibition. Moreover, I*GF2* example demonstrated that silencer removal will cause altered chromatin interaction landscape and altered histone modifications.

In the EZH2 inhibition and knockout data, we showed that MRR-associated genes as well as long-range chromatin interactions were susceptible to the depletion of H3K27me3 histone marks. The differences in the de-repression of genes associate with MRR and typical H3K27me3 peaks suggest that different genes may response differently and their response may correlate with their chromatin state. Although differences in chromatin interactions have been observed in cells at different developmental stages[51,52], whether chromatin interactions can be affected by different cell treatments is still an open question. A study in human fibroblast cells showed that the contacts between enhancers and promoters were present in the cells before the transient treatment of TNF-α[53], suggesting a pre-existing and stable chromatin architecture. However, our results suggest that long-range chromatin interactions may be affected by depletion of H3K27me3. The regulatory elements at a great distance can be brought into proximity to genes and form a permissive or repressive microenvironment around genes to help regulate their expression. To answer this question, further investigation of the structural differences in response to different cell treatments should be done using high-resolution and whole-genome chromatin interactions sequencing methods. This can help us to understand the mechanisms of gene activation or repression in cellular pathways.

The mechanism of how silencers function to repress genes will be an interesting topic to explore. Through the *IGF2* silencer example, we showed that that looping silencer removal cause distant loops to change and histone states in the

initial conditions can predict the lost loops. Importantly, we found that the initial histone state determines whether loops will change, which provides evidence that histone modifications can affect overall genome architecture. Secondly, we found that nearby loops tend to remain unchanged while long range loops are disturbed either upon silencer KO or GSK343 treatment which is in line with the finding that showed PRC1 and PRC2 are necessary to maintain the chromatin interactions landscape[17,54]. Thirdly, there are multiple regions inside an MRR that are involved in chromatin interactions and may also function as silencers. It would be interesting to see whether all the putative silencers in an MRR function differently and to dissect different functional mechanisms of silencers. Fourthly, transcription factors can contribute to the chromatin interaction landscape and cell type-specific transcription factors may result in different chromatin interaction landscape[55]. Therefore, elucidating the transcription factors involved in silencer functioning would be an important future direction for research.

We and other people found that silencers are cell-type specific and highly context-dependent[24-26] (Table S2). Specifically, for the same genomic region, they are silencers in one cell line but can be a super-enhancer in another cell line. Not surprisingly, this kind of change is associated with different gene expression. Moreover, it has been showed that silencers can transit into active enhancers during differentiation[13]. Thus, the study of relationship between cell types and silencers can shed light on cell type specific regulation of gene expression. Interestingly, we found that silencer removal leads to cell differentiation and tumor growth inhibition, which is in line with previous observed studies that showed that more H3K27me3 can render Topologically-Associated Domains (TADs) inactive and repress tumor suppressor genes[54]. It will be interesting to study the detailed mechanism of how silencers regulate tumor suppressor genes. In this way, it may be possible for us to activate the tumor suppressor genes expression by perturbing silencers, just as super-enhancer perturbation can result in loss of oncogene expression[29].

Notably, the question of whether super-enhancers are indeed different from enhancers is not settled yet[56]. Our research raises similar questions: are “super-silencers” different from typical silencers? The regions of the long MRR that are critical for silencer function are not fully elucidated yet. Here we showed that the components of the MRRs that are involved in looping interactions are important in repressing distal chromatin interactions, while the roles of other components of the MRRs are not yet known. Moreover, we found that different anchors within the same MRR can be associated with different proteins, suggesting that these different anchors may play different roles within the MRR. Detailed dissection of the different anchors and other components of MRRs will be required to answer these questions in future work.

In conclusion, maintenance of cellular identity requires that the right genes are expressed and other genes are silenced. Our results add an additional dimension to the epigenetic code by identifying silencer elements, validating the first looping silencer and deciphering its working mechanism. Just as the concept of “super-enhancers” has been useful in identifying oncogenes and therapeutic vulnerabilities in cancer cells, the concept of silencers calling by clustering of H3K27me3 may be useful in identifying genes of key cellular identity and establishment of cancer potential in the future.

Methods

We performed Hi-C interaction analysis, ChIP-seq, RNA-seq, gene expression analyses, cell culture, RT-qPCR, CRISPR excision, 4C, 3C, xenograft models, western blot, adhesion assays, and growth curves as described in the **Supplementary Methods**. A list of all libraries used and generated is provided in **Supplementary Table S3**. A list of all the primers used is provided in **Supplementary Table S4**.

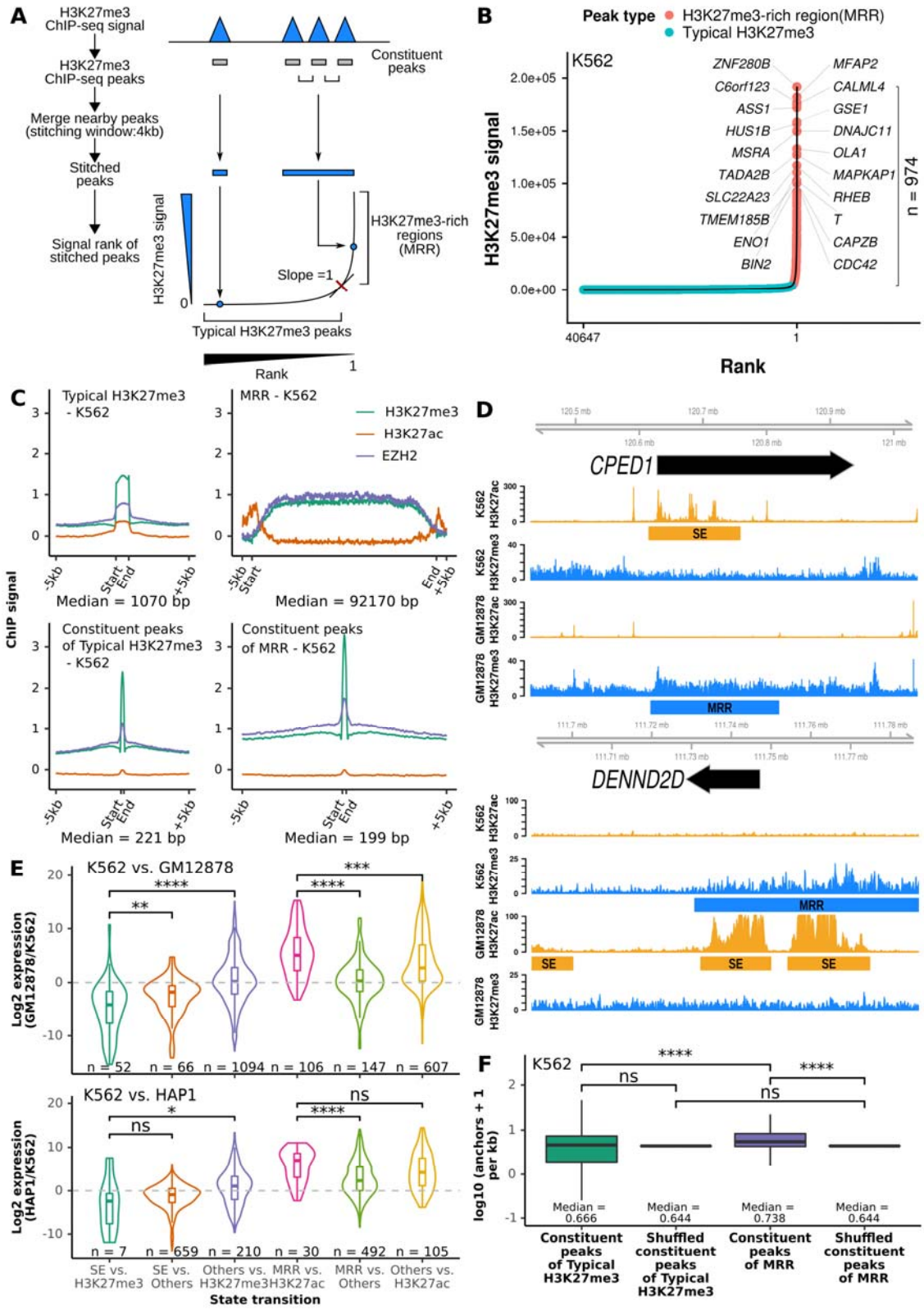

600
601
602
603

Figure 1. Definition of H3K27me3-rich regions (MRRs) and their characterization.

A. H3K27me3 ChIP-seq peaks within 4kb are stitched together and the stitched peaks ranked according to their H3K27me3 signal. The rank-ordered signal with a slope of 1 is used as cut-off for defining H3K27me3-rich MRRs. Constituent peaks are the peaks that are stitched together during the process of merging peak. **B.** H3K27me3-rich regions (MRRs) and typical H3K27me3 peaks in K562 and their associated genes. A representative overlapping gene from each of the top 10 MRRs is shown. **C.** ChIP-seq signal on typical H3K27me3, MRR, constituent peaks of typical H3K27me3 peaks, and constituent peaks of MRR regions in K562. Peaks are scaled to the same median length of peaks in typical H3K27me3 (1070 bp), MRR (92170 bp), constituent peaks of typical H3K27me3 (221 bp), or constituent peaks of MRRs (199 bp), and the plot expanded by 5kb on both sides of the peak. D**.** Example of *CPED1* and *DENND2D* and their associated MRR/SE in different cell lines. MRR and SE could be interchangeable in different cell lines. SE, super enhancers; MRR, H3K27me3-rich regions. Expression level of *CPED*1 is 107.826 and 0.029 in K562 and GM12878, respectively; expression level of *DENND2D* is 0.002 and 78.004 (expression in RPKM). E**.** Expression changes associated with different peaks between different cells. K562 vs. GM12878/K562 vs. HAP1, cell lines used in the comparison. Genes are classified based on the states of their overlapping peaks in different cell lines: [state in the first cell line] vs. [state in the second cell line], where the state can be SE, MRR, H3K27ac, H3K27me3, or Others. SE, super-enhancer; H3K27me3 peaks, either MRR or typical H3K27me3 peak; MRR, H3K27me3-rich region; H3K27ac, either super-enhancer or typical enhancer; Others, no overlapping peaks. Expression data is from Epigenetic RoadMap and in-house HAP1 RNA-seq. Wilcoxon test *p* values are as indicated. F**.** Constituent peaks of MRRs have more Hi-C interactions compared to the constituent peaks of typical H3K27me3. Constituent peaks are peaks that form super peaks as described in A. The shuffled peaks were generated by expanding the middle point of each constituent peaks to the median length of all the constituent peaks, and then followed by random genomic region shuffling. Wilcoxon test *p* values are as indicated.

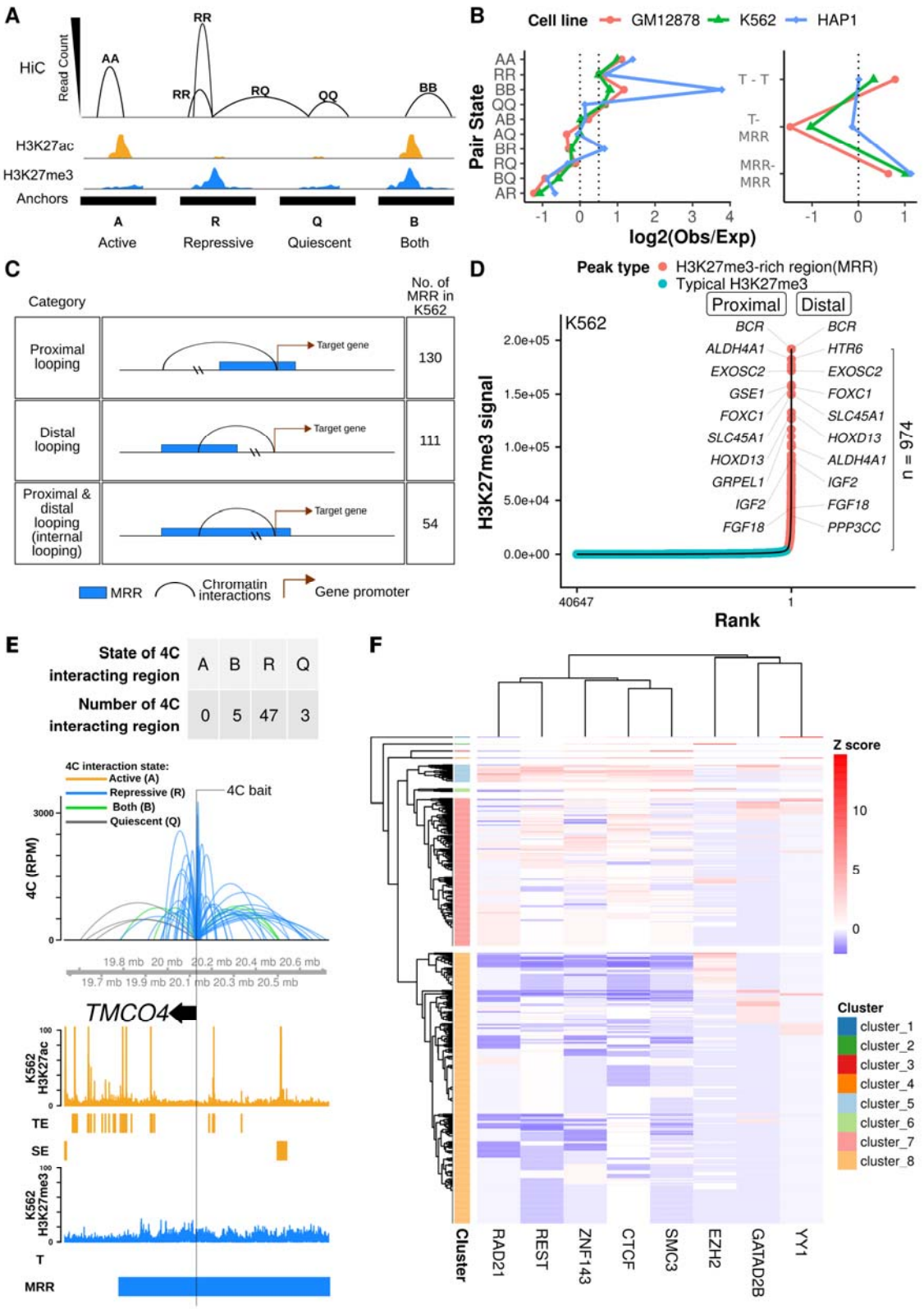

Figure 2. H3K27me3-rich regions (MRRs) preferentially associate with MRRs in the human genome via chromatin interactions.

A. Schematic plot of how different categories of Hi-C interactions are defined. Hi-C anchors are classified by whether they overlap with H3K27me3 or H3K27ac peaks. A (active), overlap with only H3K27ac peaks; R (repressive), overlap with only H3K27me3 peaks; Q (quiescent), overlap with neither H3K27ac nor H3K27me3 peaks; B (both), overlap with both H3K27ac and H3K27me3 peaks. The height of Hi-C interactions (arcs) represents the highest read counts in the interacting regions. **B.** Observed/expected ratio of Hi-C interactions in different categories. Left: categories of chromatin pair states. Right: T (typical H3K27me3) or H (MRR) peaks. The expected interactions are calculated from the marginal distributions of different anchors. **C.** Different categories of MRR associated with genes. **D.** H3K27me3-rich regions (MRRs) and typical H3K27me3 peaks in K562 and their associated genes through chromatin interactions. Peaks overlapping with Hi-C interactions are labeled with associated genes: for peaks labeled “proximal”, the gene TSS and peak occupy the same Hi-C anchor; “distal” peaks are connected to the gene via Hi-C interactions. **E.** Example of *TMCO4* 4C showing extensive internal looping within an MRR in K562. The colors of 4C interactions are based on the distal interacting regions to the 4C bait. Blue: repressive; orange: active; green: both; grey: quiescent. The state of the 4C bait is labeled by text. Each ChIP-seq tracks contains ChIP signal and peaks. TE, typical enhancer; SE, super-enhancer; T, typical H3K27me3; MRR, H3K27me3-rich region. F. Heatmap of transcription factors binding enrichment at interacting regions of MRRs. Each row represents an interacting region of MRRs (regions of MRRs that overlapped with Hi-C interactions). The number overlapping TF peaks at interacting regions are normalized to Z score per TF. Red colors indicate more binding events.

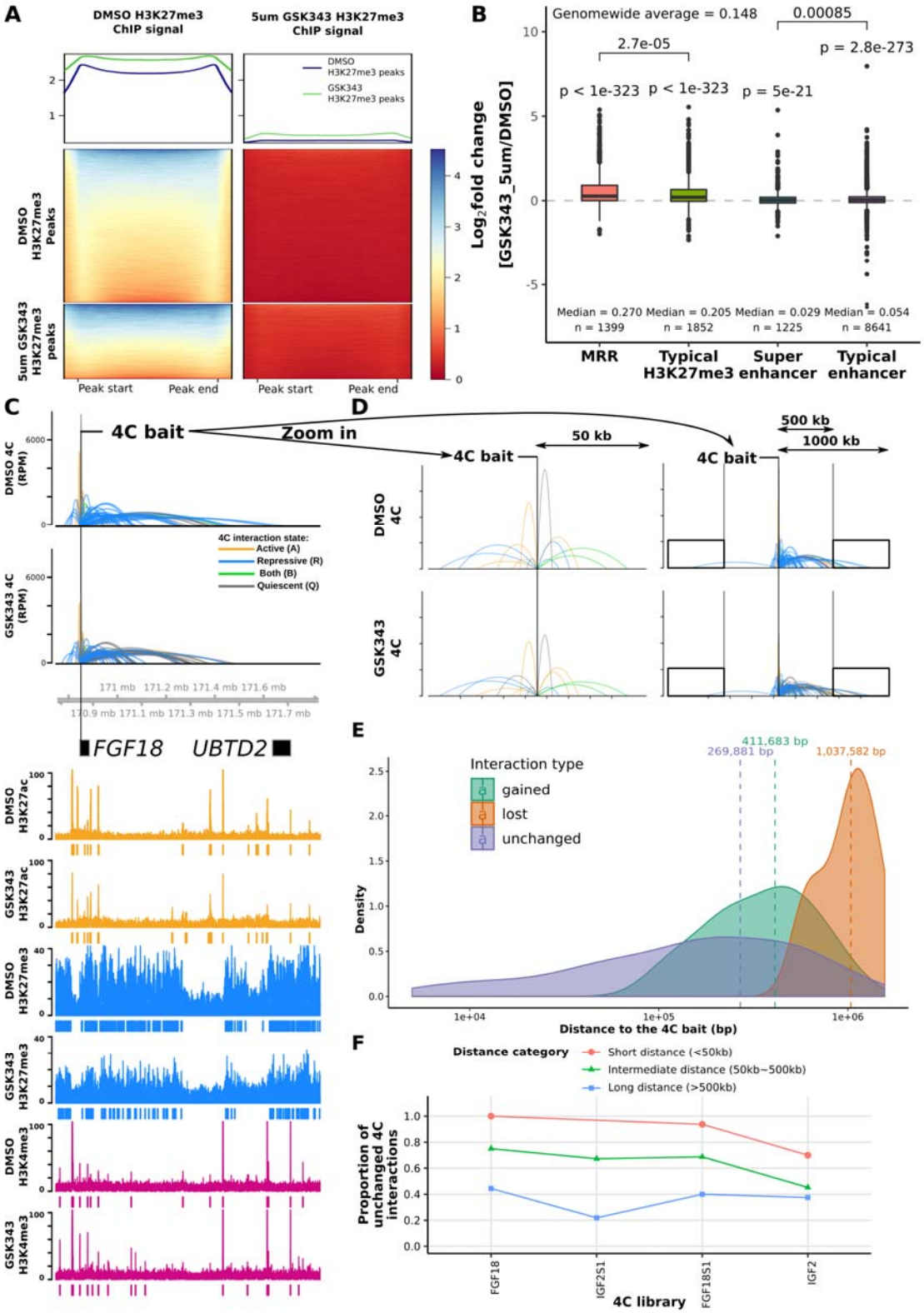
A
DMSO H3K27me3 ChIP signal
5um GSK343 H3K27me3 ChIP signal
DMSO H3K27me3 peaks
GSK343 H3K27me3 peaks
DMSO H3K27me3 Peaks
5um GSK343 H3K27me3 peaks
Peak start
Peak end
B
Genomewide average = 0.148
0.00085
2.7e-05
p = 2.8e-273
p < 1e-323
p < 1e-323
p = 5e-21
Log2fold change [GSK343_5um/DMSO]
Median = 0.270 n = 1399
Median = 0.205 n = 1852
Median = 0.029 n = 1225
Median = 0.054 n = 8641
MRR
Typical H3K27me3
Super enhancer
Typical enhancer
C
4C bait
Zoom in
DMSO 4C (RPM)
GSK343 4C (RPM)
4C interaction state:
Active (A)
Repressive (R)
Both (B)
Quiescent (Q)
171 mb 171.2 mb 171.4 mb 171.6 mb
170.9 mb 171.1 mb 171.3 mb 171.5 mb 171.7 mb
FGF18 UBTD2
DMSO H3K27ac
GSK343 H3K27ac
DMSO H3K27me3
GSK343 H3K27me3
DMSO H3K4me3
GSK343 H3K4me3
D
4C bait
50 kb
500 kb
1000 kb
DMSO 4C
GSK343 4C
E
Interaction type
gained
lost
unchanged
411,683 bp
269,881 bp
1,037,582 bp
Density
Distance to the 4C bait (bp)
F
Distance category
Short distance (<50kb)
Intermediate distance (50kb~500kb)
Long distance (>500kb)
Proportion of unchanged 4C interactions
FGF18
IGF2S1
FGF18S1
IGF2
4C library

709
710
711

Figure 3. MRR-associated gene expression and long-range chromatin interactions to EZH2 perturbation.

A. H3K27me3 ChIP-seq signal at peaks from DMSO-treated and 5μm GSK343-treated K562 cells. **B.** Expression changes of genes associated with different types of peaks in 5μm GSK343-treated K562 cells. Genes included: 1) Genes with TSS overlapped with different peaks; 2) Genes associated with different peaks through Hi-C interaction. One-tail wald test was used for testing significantly up-regulation. All the P values of genes in each category are aggregated. **C.** 4C results of *FGF18* in DMSO and GSK343-treated K562 cells. The colors of 4C interactions are based on the distal interacting regions to the 4C bait. Blue: repressive; orange: active; green: both; grey: quiescent. The height of the 4C is shown in Reads Per Million (RPM). The ChIP signal and peaks of H3K27ac, H3K27me3, and H3K4me3 are shown. **D**. Close up view of 4C interactions at 50 kb (left) and 1000 kb range (right). The color of 4C interactions are the same as in C. Highlighted regions have changed in 4C interactions after EZH2 inhibition treatment. **E**. Density plot of different categories of 4C interactions on the same chromosome as the bait. All the 4C interactions that have p-value < 0.05 on the same chromosome as the 4C bait are included. Gained, 4C interactions present in GSK343-treated 4C but not DMSO-treated 4C; lost, 4C interaction present in DMSO-treated 4C but not GSK343-treated 4C; unchanged, 4C interactions present in both DMSO-treated and GSK343-treated 4C. Mean distances of each category are indicated by vertical dashed line. **F**. Proportions of unchanged 4C interactions in different distance categories in 5μm GSK343-treated K562 cells. The proportions were calculated separately for each distance category (short distance, intermediate distance, and long distance). As the distance of 4C interactions increases, the proportion of unchanged 4C interactions drops, suggesting that long-range interactions are perturbed.

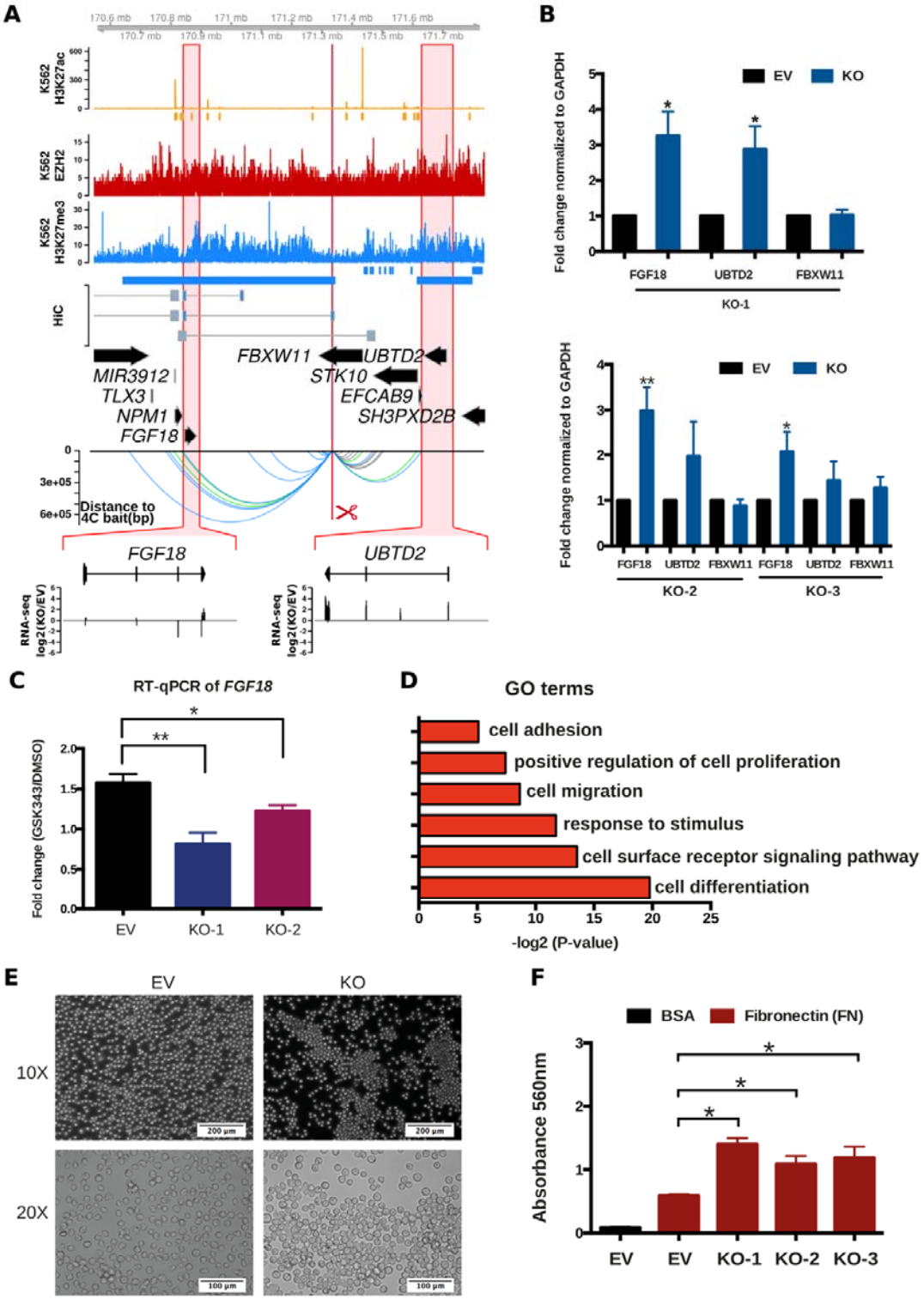

745
746
747
748

Figure 4. CRISPR excision of a silencer looping to *FGF18* leads to *FGF18* gene upregulation and altered cell adhesion.

A. Screenshot showing EZH2 ChIP-seq, H3K27me3 ChIP-seq, H3K27ac ChIP-seq and chromatin interactions as identified from previously published Hi-C data[22], gene information, and 4C performed on the CRISPR-excised region in wild-type cells confirming chromatin interactions to *FGF18*, as well as showing chromatin interactions to *UBTD2*. The regions highlighted in the red boxes are shown in more detail, with RNA-seq was shown as one CRISPR knockout clone over wild-type at *FGF18* and *UBTD2*. The blue bar shows the predicted whole MRR. The red box with the red scissors indicates the region which was excised. **B.** RT-qPCR of *FGF18*, *UBTD2* and *FBXW11* in three different CRISPR-excised clones (KO-1, KO-2, KO-3) as compared with vector control cells ("Empty Vector", "EV"). **C.** RT-qPCR of *FGF18* expression upon GSK343 treatment in EV cells and two KO cells (KO-1 and KO-2). **D.** Gene Ontology (GO) was performed using significant DE genes in the RNA-seq data which was shown as $-\log_2$(p value). **E.** Light microscopy photos of empty vector (EV) and CRISPR knockout cells (KO) showing increased cell adhesion and aggregates in the KO clones. 10X and 20X magnification were shown. **F.** A fibronectin adhesion assay showed increased adhesion of the three CRISPR knockout cells (KO) as compared with empty vector (EV). BSA was used as a negative control. All data shown here are average + standard error. P value less than 0.05 is shown as *. P value less than 0.01 is shown as **.

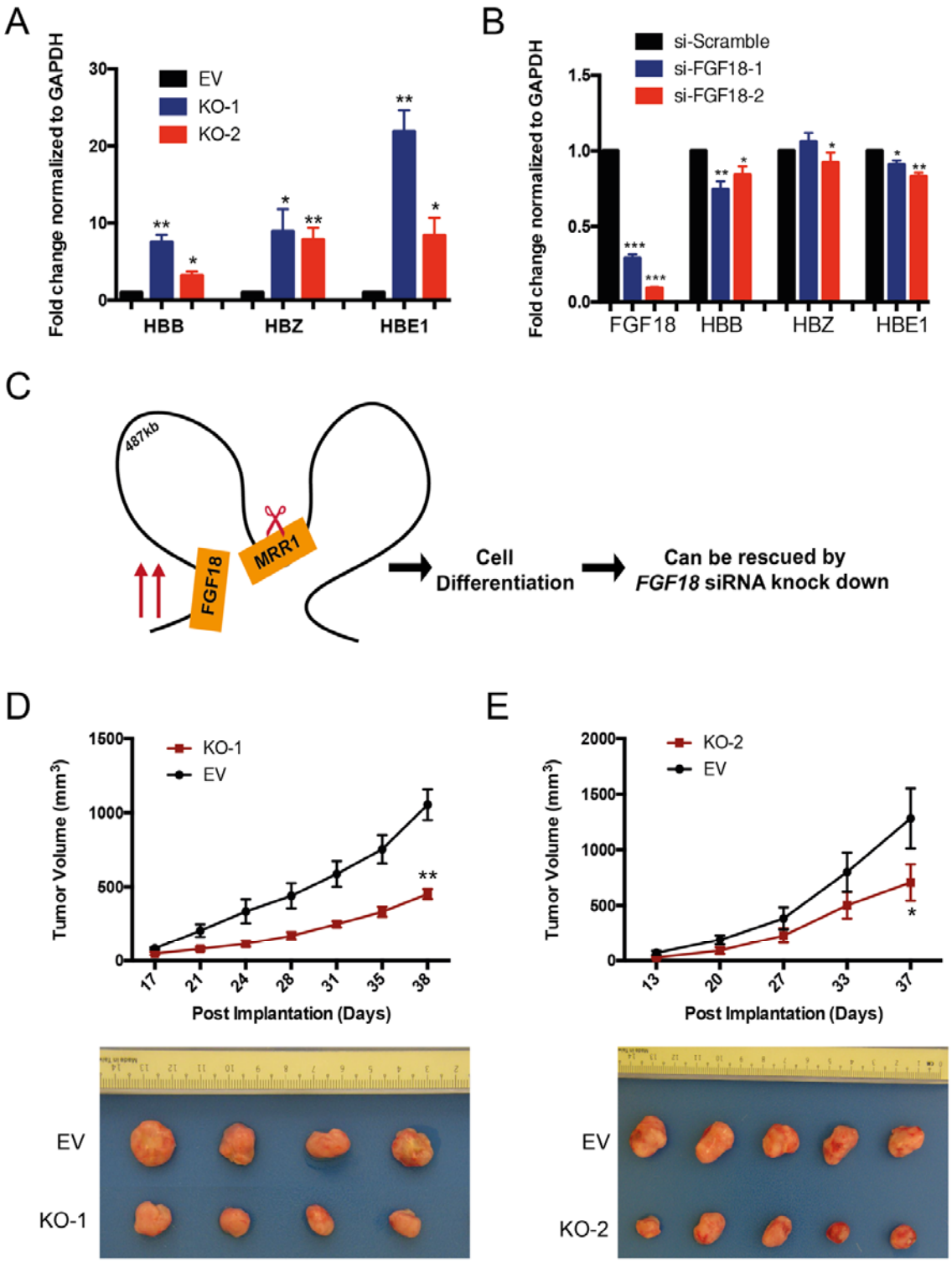
A
Fold change normalized to GAPDH
EV
KO-1
KO-2
HBB
HBZ
HBE1
B
si-Scramble
si-FGF18-1
si-FGF18-2
FGF18
HBB
HBZ
HBE1
C
487kb
FGF18
MRR1
Cell Differentiation
Can be rescued by FGF18 siRNA knock down
D
Tumor Volume (mm3)
KO-1
EV
Post Implantation (Days)
E
KO-2
EV
Post Implantation (Days)
EV
KO-1
EV
KO-2

794
795
796

Figure 5. CRISPR excision of an silencer looping to *FGF18* leads to erythroid differentiation and tumor growth inhibition.

A. RT-qPCR of hemoglobin genes (*HBB*, *HBZ* and *HBE1*) in EV and two KO cells. **B.** RT-qPCR of hemoglobin genes (*HBB*, *HBZ* and *HBE1*) upon *FGF18* siRNA knock down in KO cells. **C**. Cartoon schematic summary of the *FGF18* looping silencer. **D&E**. Tumor growth in SCID (Severe Combined Immunodeficiency) mice injected with MRR1-A1 knock out cells and empty vector cells (EV). The upper panel shows the tumor growth curve, and data shown as tumor volume with different post implantation days. The panel below was representative tumor picture at the final day. All data shown here are average + standard error. P value less than 0.05 is shown as *. P value less than 0.01 is shown as **.

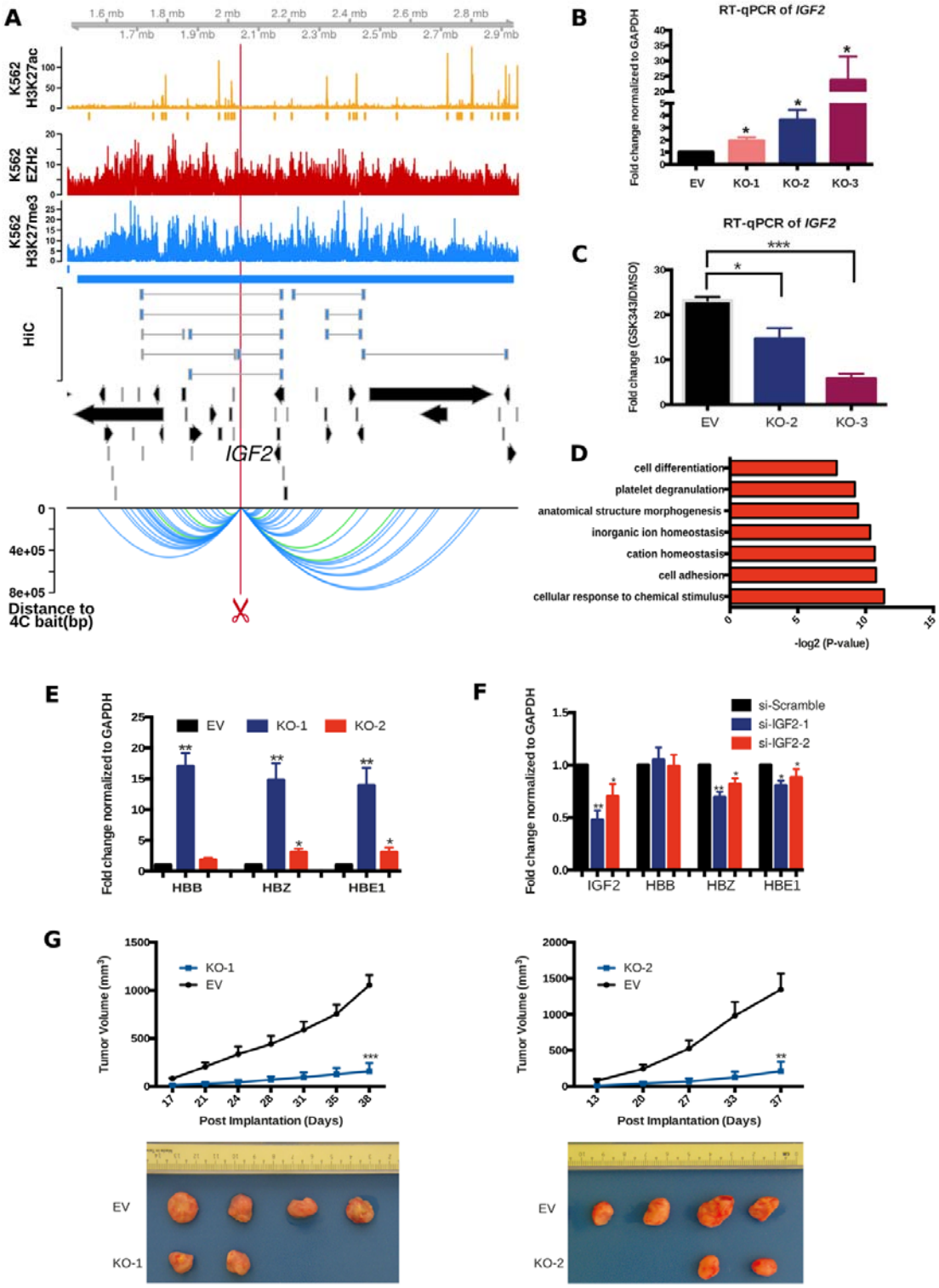

808
809
810
811
812

Figure 6. CRISPR excision of a silencer looping to *IGF2* leads to *IGF2* gene upregulation, erythroid differentiation and tumor growth inhibition.

A. Screenshot showing EZH2 ChIP-seq, H3K27me3 ChIP-seq, H3K27ac ChIP-seq and chromatin interactions as identified from previously published Hi-C data[22], gene information, and 4C performed on the CRISPR-excised region in wild-type cells confirming chromatin interactions to *IGF2*. The blue bar shows the predicted whole MRR. The red box with the red scissors indicates the region which was excised. **B.** RT-qPCR of *IGF2* in three different CRISPR-excised clones (KO-1, KO-2, KO-3) as compared with vector control cells ("EV"). **C.** RT-qPCR of *IGF2* expression upon GSK343 treatment in EV cells and two KO cells (KO-1 and KO-2). **D.** Gene Ontology (GO) was performed using significant DE genes in the RNA-seq data shown as –log2(p value). **E.** RT-qPCR of hemoglobin genes (*HBB*, *HBZ* and *HBE1*) in EV and two KO cells. **F.** RT-qPCR of hemoglobin genes (*HBB*, *HBZ* and *HBE1*) upon *IGF2* siRNA knock down in KO cells. **G**. Tumor growth in SCID (Severe Combined Immunodeficiency) mice injected with MRR2-A1 knock out cells and empty vector cells (EV). The upper panel shows the tumor growth curve, and data shown as tumor volume with different post implantation days. The panel below was representative tumor picture at the final day. All data shown here are average + standard error. P value less than 0.05 is shown as *. P value less than 0.01 is shown as **. P value less than 0.001 is shown as ***.

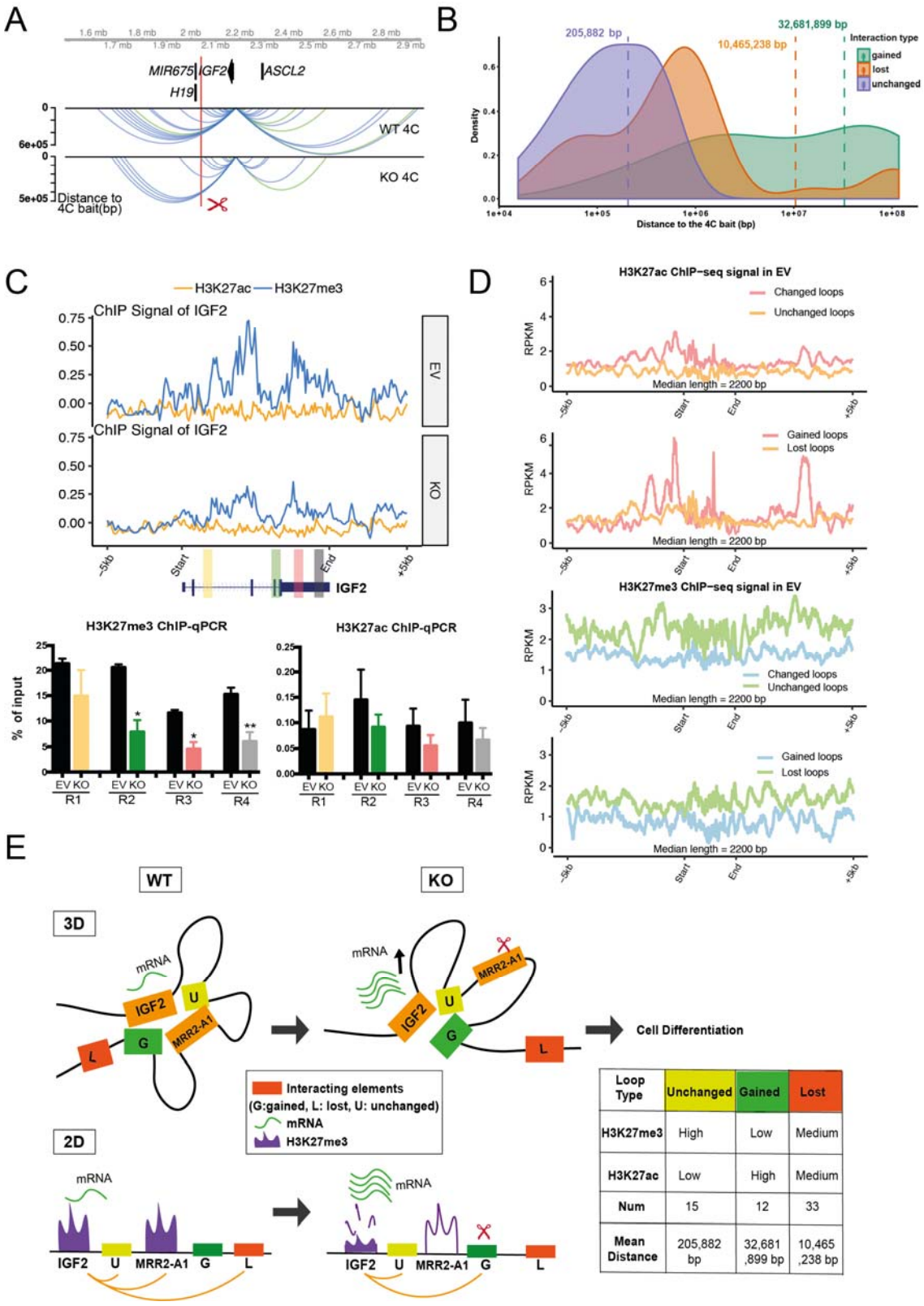

Loop Type	Unchanged	Gained	Lost
H3K27me3	High	Low	Medium
H3K27ac	Low	High	Medium
Num	15	12	33
Mean Distance	205,882 bp	32,681 ,899 bp	10,465 ,238 bp

Figure 7. Initial histone states determine the changed loops upon IGF2 silencer removal.

A. Representative chromatin interactions at *IGF2* bait in KO cells and control cells which shown as loops. **B**. The average distance of changed loops (gained loops and lost loops) is greater than unchanged loops. **C**. ChIP-seq and ChIP-qPCR of H3K27me3 and H3K27ac for four regions (R1-R4) at *IGF2* gene in EV and KO cells. Data shown here are average + standard error. P value less than 0.05 is shown as *. P value less than 0.01 is shown as **. **D**. Integrative analysis of ChIP-seq (H3K27me3 and H3K27ac) and 4C-seq at *IGF2* bait showed the characteristic of three loop categories: unchanged loops, gained loops and lost loops. **E**. 3D and 2D model showing *IGF2* looping silencer removal caused distant loops to change and that initial histone states are associated with changed loops.

Acknowledgements

We would like to thank all members of the Fullwood Lab and Ah Jung Jeon for helpful comments. This research is supported by the National Research Foundation (NRF) Singapore through an NRF Fellowship awarded to M.J.F (NRF-NRFF2012-054) and NTU start-up funds awarded to M.J.F. This research is supported by the RNA Biology Center at the Cancer Science Institute of Singapore, NUS, as part of funding under the Singapore Ministry of Education Academic Research Fund Tier 3 awarded to Daniel Tenen (MOE2014-T3-1-006). This research is supported by an Singapore MOE Academic Research Research Fund (T1) grant to G.T-K. This research is supported by the National Research Foundation Singapore and the Singapore Ministry of Education under its Research Centres of Excellence initiative.

Author contributions

Y.C.C., Y.Z., M.J.F. and G.T-K. conceived of the research. Y.C.C., Y.Z., M.J.F. and G.T-K. contributed to the study design. Y.C.C. performed bioinformatics analysis. Y.Z. and S.L. designed CRISPR knock out experiments. Y.Z. performed CRISPR knock out, 4C, RNA-seq, ChIP-seq, ChIP-qPCR and other functional experiments for KO cells. Y.P.L. performed EZH2 inhibitor and HAP1 *EZH2* knockout experiments and 4C experiments. J.Q.T performed ChIP-seq and ChIP-qPCR experiments for HAP1 EZH2 KO cells. Z.C. and M.Q.L. performed 4C experiments. A.R., L.M. and V.T. designed xenograft experiments. A.R. performed xenograft experiments. Y.C.C., Y.Z., M.J.F. and G.T-K. reviewed the data and wrote the manuscript. All authors reviewed and approved of the manuscript.

Data deposition

The list of libraries used in the study is provided in Table S3. All datasets have been deposited into GEO.

Author information

The authors declare that they have no competing interests.

Correspondence and requests for materials should be addressed to mfullwood@ntu.edu.sg and dbsgtk@nus.edu.sg.

References

1 Schmitt, A. D., Hu, M. & Ren, B. Genome-wide mapping and analysis of chromosome architecture. *Nat Rev Mol Cell Biol* **17**, 743-755, doi:10.1038/nrm.2016.104 (2016).

2 See, Y. X., Wang, B. Z. & Fullwood, M. J. Chromatin Interactions and Regulatory Elements in Cancer: From Bench to Bedside. *Trends Genet* **35**, 145-158, doi:10.1016/j.tig.2018.11.007 (2019).

3 Babu, D. & Fullwood, M. J. 3D genome organization in health and disease: emerging opportunities in cancer translational medicine. *Nucleus* **6**, 382-393, doi:10.1080/19491034.2015.1106676 (2015).

4 Bradner, J. E., Hnisz, D. & Young, R. A. Transcriptional Addiction in Cancer. *Cell* **168**, 629-643, doi:10.1016/j.cell.2016.12.013 (2017).

5 Akincilar, S. C. *et al.* Long-Range Chromatin Interactions Drive Mutant TERT Promoter Activation. *Cancer Discov* **6**, 1276-1291, doi:10.1158/2159-8290.CD-16-0177 (2016).

6 Li, L., Suzuki, T., Mori, N. & Greengard, P. Identification of a functional silencer element involved in neuron-specific expression of the synapsin I gene. *Proc Natl Acad Sci U S A* **90**, 1460-1464 (1993).

7 Zuccato, C. *et al.* Widespread disruption of repressor element-1 silencing transcription factor/neuron-restrictive silencer factor occupancy at its target genes in Huntington's disease. *J Neurosci* **27**, 6972-6983, doi:10.1523/JNEUROSCI.4278-06.2007 (2007).

8 Donda, A., Schulz, M., Burki, K., De Libero, G. & Uematsu, Y. Identification and characterization of a human CD4 silencer. *Eur J Immunol* **26**, 493-500, doi:10.1002/eji.1830260232 (1996).

9 Sawada, S., Scarborough, J. D., Killeen, N. & Littman, D. R. A lineage-specific transcriptional silencer regulates CD4 gene expression during T lymphocyte development. *Cell* **77**, 917-929, doi:10.1016/0092-8674(94)90140-6 (1994).

10 Kolovos, P., Knoch, T. A., Grosveld, F. G., Cook, P. R. & Papantonis, A. Enhancers and silencers: an integrated and simple model for their function. *Epigenetics Chromatin* **5**, 1, doi:10.1186/1756-8935-5-1 (2012).

11 Mifsud, B. *et al.* Mapping long-range promoter contacts in human cells with high-resolution capture Hi-C. *Nat Genet* **47**, 598-606, doi:10.1038/ng.3286 (2015).

12 Eagen, K. P., Aiden, E. L. & Kornberg, R. D. Polycomb-mediated chromatin loops revealed by a subkilobase-resolution chromatin interaction map. *Proc Natl Acad Sci U S A* **114**, 8764-8769, doi:10.1073/pnas.1701291114 (2017).

13 Ngan, C. Y. *et al.* Chromatin interaction analyses elucidate the roles of PRC2-bound silencers in mouse development. *Nat Genet* **52**, 264-272, doi:10.1038/s41588-020-0581-x (2020).

14 Muller, J. Transcriptional silencing by the Polycomb protein in Drosophila embryos. *EMBO J* **14**, 1209-1220 (1995).

15 Margueron, R. & Reinberg, D. The Polycomb complex PRC2 and its mark in life. *Nature* **469**, 343-349, doi:10.1038/nature09784 (2011).

16 Schuettengruber, B. & Cavalli, G. Polycomb domain formation depends on short and long distance regulatory cues. *PLoS One* **8**, e56531, doi:10.1371/journal.pone.0056531 (2013).

17 Schoenfelder, S. *et al.* Polycomb repressive complex PRC1 spatially constrains the mouse embryonic stem cell genome. *Nat Genet* **47**, 1179-1186, doi:10.1038/ng.3393 (2015).

18 Kundu, S. *et al.* Polycomb Repressive Complex 1 Generates Discrete Compacted Domains that Change during Differentiation. *Mol Cell* **65**, 432-446 e435, doi:10.1016/j.molcel.2017.01.009 (2017).
19 Schuettengruber, B. & Cavalli, G. Recruitment of polycomb group complexes and their role in the dynamic regulation of cell fate choice. *Development* **136**, 3531-3542, doi:10.1242/dev.033902 (2009).
20 Nakagawa, M. & Kitabayashi, I. Oncogenic roles of enhancer of zeste homolog 1/2 in hematological malignancies. *Cancer Sci* **109**, 2342-2348, doi:10.1111/cas.13655 (2018).
21 Soufi, A., Donahue, G. & Zaret, K. S. Facilitators and impediments of the pluripotency reprogramming factors' initial engagement with the genome. *Cell* **151**, 994-1004, doi:10.1016/j.cell.2012.09.045 (2012).
22 Bernstein, B. E. *et al.* A bivalent chromatin structure marks key developmental genes in embryonic stem cells. *Cell* **125**, 315-326, doi:10.1016/j.cell.2006.02.041 (2006).
23 Hosogane, M., Funayama, R., Shirota, M. & Nakayama, K. Lack of Transcription Triggers H3K27me3 Accumulation in the Gene Body. *Cell Rep* **16**, 696-706, doi:10.1016/j.celrep.2016.06.034 (2016).
24 Huang, D., Petrykowska, H. M., Miller, B. F., Elnitski, L. & Ovcharenko, I. Identification of human silencers by correlating cross-tissue epigenetic profiles and gene expression. *Genome Res* **29**, 657-667, doi:10.1101/gr.247007.118 (2019).
25 Doni Jayavelu, N., Jajodia, A., Mishra, A. & Hawkins, R. D. An atlas of silencer elements for the human and mouse genomes. *bioRxiv*, 252304, doi:10.1101/252304 (2018).
26 Pang, B. & Snyder, M. P. Systematic identification of silencers in human cells. *Nat Genet* **52**, 254-263, doi:10.1038/s41588-020-0578-5 (2020).
27 Hnisz, D. *et al.* Super-enhancers in the control of cell identity and disease. *Cell* **155**, 934-947, doi:10.1016/j.cell.2013.09.053 (2013).
28 Wang, X., Cairns, M. J. & Yan, J. Super-enhancers in transcriptional regulation and genome organization. *Nucleic Acids Res* **47**, 11481-11496, doi:10.1093/nar/gkz1038 (2019).
29 Loven, J. *et al.* Selective inhibition of tumor oncogenes by disruption of super-enhancers. *Cell* **153**, 320-334, doi:10.1016/j.cell.2013.03.036 (2013).
30 Hnisz, D. *et al.* Super-enhancers in the control of cell identity and disease. *Cell* **155**, 934-947, doi:10.1016/j.cell.2013.09.053 (2013).
31 Pott, S. & Lieb, J. D. What are super-enhancers? *Nat Genet* **47**, 8-12, doi:10.1038/ng.3167 (2015).
32 Consortium, E. P. An integrated encyclopedia of DNA elements in the human genome. *Nature* **489**, 57-74, doi:10.1038/nature11247 (2012).
33 Whyte, W. A. *et al.* Master transcription factors and mediator establish super-enhancers at key cell identity genes. *Cell* **153**, 307-319, doi:10.1016/j.cell.2013.03.035 (2013).
34 Davoli, T. *et al.* Cumulative haploinsufficiency and triplosensitivity drive aneuploidy patterns and shape the cancer genome. *Cell* **155**, 948-962, doi:10.1016/j.cell.2013.10.011 (2013).
35 Kunchala, P., Kuravi, S., Jensen, R., McGuirk, J. & Balusu, R. When the good go bad: Mutant NPM1 in acute myeloid leukemia. *Blood Rev* **32**, 167-183, doi:10.1016/j.blre.2017.11.001 (2018).

36 Ziai, J. M., Siddon, A. J., Education Committee of the Academy of Clinical Laboratory, P. & Scientists. Pathology Consultation on Gene Mutations in Acute Myeloid Leukemia. *Am J Clin Pathol* **144**, 539-554, doi:10.1309/AJCP77ZFPUQGYGWY (2015).
37 Sportoletti, P. *et al.* Npm1 is a haploinsufficient suppressor of myeloid and lymphoid malignancies in the mouse. *Blood* **111**, 3859-3862, doi:10.1182/blood-2007-06-098251 (2008).
38 Hirsch, S. *et al.* Circular RNAs of the nucleophosmin (NPM1) gene in acute myeloid leukemia. *Haematologica* **102**, 2039-2047, doi:10.3324/haematol.2017.172866 (2017).
39 Messina, M. *et al.* Genetic lesions associated with chronic lymphocytic leukemia chemo-refractoriness. *Blood* **123**, 2378-2388, doi:10.1182/blood-2013-10-534271 (2014).
40 de Bock, C. E. *et al.* The Fat1 cadherin is overexpressed and an independent prognostic factor for survival in paired diagnosis-relapse samples of precursor B-cell acute lymphoblastic leukemia. *Leukemia* **26**, 918-926, doi:10.1038/leu.2011.319 (2012).
41 Rao, S. S. *et al.* A 3D map of the human genome at kilobase resolution reveals principles of chromatin looping. *Cell* **159**, 1665-1680, doi:10.1016/j.cell.2014.11.021 (2014).
42 Cao, F. *et al.* Super-Enhancers and Broad H3K4me3 Domains Form Complex Gene Regulatory Circuits Involving Chromatin Interactions. *Sci Rep* **7**, 2186, doi:10.1038/s41598-017-02257-3 (2017).
43 Shimokawa, T. *et al.* Involvement of the FGF18 gene in colorectal carcinogenesis, as a novel downstream target of the beta-catenin/T-cell factor complex. *Cancer Res* **63**, 6116-6120 (2003).
44 Jeon, E. *et al.* Investigating the role of FGF18 in the cultivation and osteogenic differentiation of mesenchymal stem cells. *PLoS One* **7**, e43982, doi:10.1371/journal.pone.0043982 (2012).
45 Constancia, M. *et al.* Placental-specific IGF-II is a major modulator of placental and fetal growth. *Nature* **417**, 945-948, doi:10.1038/nature00819 (2002).
46 Ravenel, J. D. *et al.* Loss of imprinting of insulin-like growth factor-II (IGF2) gene in distinguishing specific biologic subtypes of Wilms tumor. *J Natl Cancer Inst* **93**, 1698-1703, doi:10.1093/jnci/93.22.1698 (2001).
47 Bruecher-Encke, B., Griffin, J. D., Neel, B. G. & Lorenz, U. Role of the tyrosine phosphatase SHP-1 in K562 cell differentiation. *Leukemia* **15**, 1424-1432, doi:10.1038/sj.leu.2402214 (2001).
48 Huang, R. *et al.* Megakaryocytic differentiation of K562 cells induced by PMA reduced the activity of respiratory chain complex IV. *PLoS One* **9**, e96246, doi:10.1371/journal.pone.0096246 (2014).
49 Ma, Y. N. *et al.* Emodin can induce K562 cells to erythroid differentiation and improve the expression of globin genes. *Mol Cell Biochem* **382**, 127-136, doi:10.1007/s11010-013-1726-3 (2013).
50 Ogino, T., Kobuchi, H., Fujita, H., Matsukawa, A. & Utsumi, K. Erythroid and megakaryocytic differentiation of K562 erythroleukemic cells by monochloramine. *Free Radic Res* **48**, 292-302, doi:10.3109/10715762.2013.865840 (2014).

51 Li, G. *et al.* Extensive promoter-centered chromatin interactions provide a topological basis for transcription regulation. *Cell* **148**, 84-98, doi:10.1016/j.cell.2011.12.014 (2012).
52 Kieffer-Kwon, K. R. *et al.* Interactome maps of mouse gene regulatory domains reveal basic principles of transcriptional regulation. *Cell* **155**, 1507-1520, doi:10.1016/j.cell.2013.11.039 (2013).
53 Jin, F. *et al.* A high-resolution map of the three-dimensional chromatin interactome in human cells. *Nature* **503**, 290-294, doi:10.1038/nature12644 (2013).
54 Donaldson-Collier, M. C. *et al.* EZH2 oncogenic mutations drive epigenetic, transcriptional, and structural changes within chromatin domains. *Nat Genet* **51**, 517-528, doi:10.1038/s41588-018-0338-y (2019).
55 Bonev, B. *et al.* Multiscale 3D Genome Rewiring during Mouse Neural Development. *Cell* **171**, 557-572 e524, doi:10.1016/j.cell.2017.09.043 (2017).
56 Huang, J. *et al.* Dissecting super-enhancer hierarchy based on chromatin interactions. *Nat Commun* **9**, 943, doi:10.1038/s41467-018-03279-9 (2018).